AD-A112 238 AEROSPACE CORP EL SEGUNDO CA MATERIALS SCIENCES LAB F/G 14/2
ANALYSIS AND DESIGN OF A NEW PHASE-MODULATED MICHELSON INTERFER--ETC(U)
DEC 81 S A ESELUN, R C SAVEDRA, E B WOLFF F04701-81-C-0082
UNCLASSIFIED TR-0082(2935-07)-1 SD-TR-81-113 NL

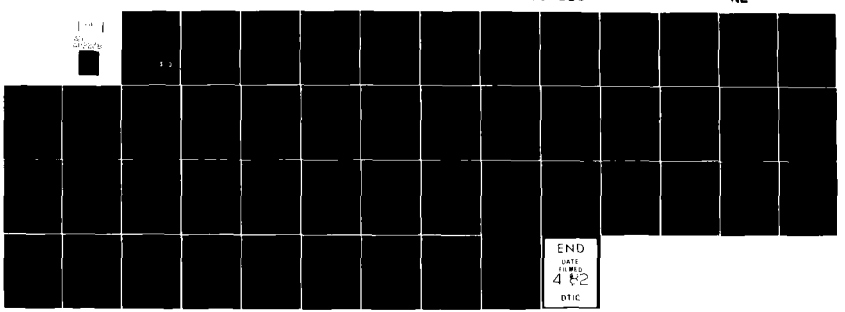

END
DATE FILMED
4 82
DTIC

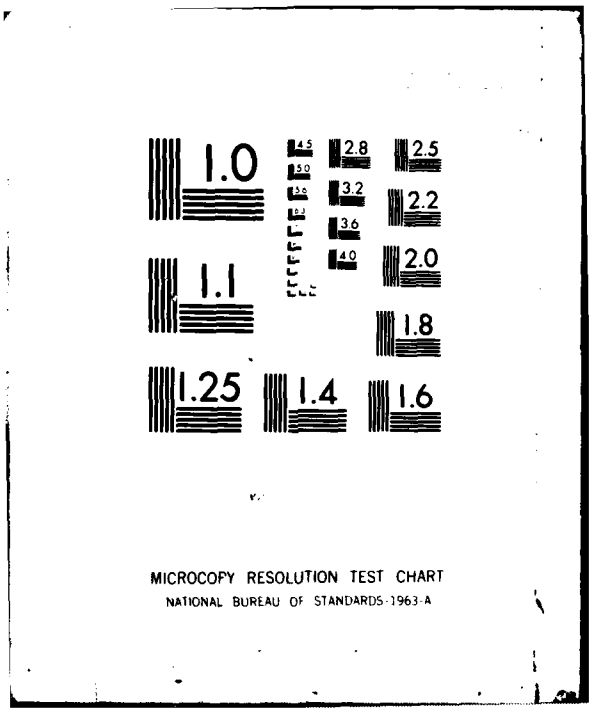
1.0
1.1
1.25
1.4
1.6
1.8
2.0
2.2
2.5
2.8
3.2
3.6
4.0
4.5
5.0
5.6
MICROCOPY RESOLUTION TEST CHART
NATIONAL BUREAU OF STANDARDS-1963-A

REPORT SD-TR-81-113

(12)

Analysis and Design of a New Phase-Modulated Michelson Interferometer

S. A. ESELUN, R. C. SAVEDRA,
and E. G. WOLFF
Materials Sciences Laboratory
Laboratory Operations
The Aerospace Corporation
El Segundo, Calif. 90245

18 December 1981

Prepared for

SPACE DIVISION
AIR FORCE SYSTEMS COMMAND
Los Angeles Air Force Station
P.O. Box 92960, Worldway Postal Center
Los Angeles, Calif. 90009

This report was submitted by The Aerospace Corporation, El Segundo, CA 90245, under Contract No. F04701-81-C-0082 with the Space Division, Deputy for Technology, P.O. Box 92960, Worldway Postal Center, Los Angeles, CA 90009. It was reviewed and approved for The Aerospace Corporation by W. C. Riley, Director, Materials Sciences Laboratory. Major Ralph R. Gajewski, SD/YLXT, was the project officer for the Mission-Oriented Investigation and Experimentation (MOIE) Programs.

This report has been reviewed by the Public Affairs Office (PAS) and is releasable to the National Technical Information Service (NTIS). At NTIS, it will be available to the general public, including foreign nations.

This technical report has been reviewed and is approved for publication. Publication of this report does not constitute Air Force approval of the report's findings or conclusions. It is published only for the exchange and stimulation of ideas.

Ralph R. Gajewski
Ralph R. Gajewski, Major, USAF
Project Officer

Florian P. Meinhardt
Florian P. Meinhardt, Lt Col, USAF
Director of Advanced Space Development

FOR THE COMMANDER

Norman W. Lee
Norman W. Lee, Jr., Colonel, USAF
Deputy for Technology

UNCLASSIFIED

SECURITY CLASSIFICATION OF THIS PAGE *(When Data Entered)*

REPORT DOCUMENTATION PAGE	READ INSTRUCTIONS BEFORE COMPLETING FORM
1. REPORT NUMBER: SD-TR-81-113	2. GOVT ACCESSION NO.: AD-A113223
3. RECIPIENT'S CATALOG NUMBER:	
4. TITLE *(and Subtitle)*: ANALYSIS AND DESIGN OF A NEW PHASE-MODULATED MICHELSON INTERFEROMETER	5. TYPE OF REPORT & PERIOD COVERED:
	6. PERFORMING ORG. REPORT NUMBER: TR-0082(2935-07)-1
7. AUTHOR(s): S. A. Eselun, R. C. Savedra, and E. G. Wolff	8. CONTRACT OR GRANT NUMBER(s): F04701-81-C-0082
9. PERFORMING ORGANIZATION NAME AND ADDRESS: The Aerospace Corporation, El Segundo, Calif. 90245	10. PROGRAM ELEMENT, PROJECT, TASK AREA & WORK UNIT NUMBERS:
11. CONTROLLING OFFICE NAME AND ADDRESS: Space Division, Air Force Systems Command, Los Angeles, Calif. 90009	12. REPORT DATE: 18 December 1981
	13. NUMBER OF PAGES: 44
14. MONITORING AGENCY NAME & ADDRESS *(if different from Controlling Office)*:	15. SECURITY CLASS. *(of this report)*: Unclassified
	15a. DECLASSIFICATION/DOWNGRADING SCHEDULE:

16. DISTRIBUTION STATEMENT *(of this Report)*

Approved for public release; distribution unlimited

17. DISTRIBUTION STATEMENT *(of the abstract entered in Block 20, if different from Report)*

18. SUPPLEMENTARY NOTES

19. KEY WORDS *(Continue on reverse side if necessary and identify by block number)*

Dimensional Stability
Fringe Analysis
Interferometer
Phase Modulation
Signal Processing

20. ABSTRACT *(Continue on reverse side if necessary and identify by block number)*

A new interferometer signal processing system has been designed, analyzed, constructed, and tested. It is based on phase modulation of the interferometer followed electronically by quadrature mixing and frequency-modulated (FM)-type detection. As a result, the system is entirely independent of direct current (dc) or polarization effects, and only one photodetector is required to provide directional information. The output is digital and analog. The range of the unit with two 8-bit counters is presently ±64 λ;

DD FORM 1473 (FACSIMILE)

UNCLASSIFIED

SECURITY CLASSIFICATION OF THIS PAGE *(When Data Entered)*

19. KEY WORDS (Continued)

20. ABSTRACT (Continued)

however, more counters could be combined to provide a total ΔL to the beam coherence length. The unit will detect signals to 30 kHz. Resolution through fringe interpolation is possible to $\pm\lambda/95$ at present, which can be improved with electronic modifications. Phase sensitivity is much greater, with about 3-μV signal per angstrom of length change.

CONTENTS

I. INTRODUCTION..... 5

II. THEORY..... 7

A. Michelson Interferometer..... 7

B. Modulation Methods..... 9

III. ANALYSIS..... 13

A. Signal Processing..... 13

B. Measurement of Depth of Modulation..... 16

IV. DESIGN..... 25

A. Circuitry..... 25

B. Fringe Counting and Phase Interpolation..... 25

C. Distortion Analysis..... 28

V. PERFORMANCE..... 29

A. Resolution..... 29

B. Frequency Response..... 29

C. Thermal Expansion Testing..... 33

VI. DISCUSSION..... 35

REFERENCES..... 37

APPENDIX: CIRCUIT DIAGRAMS..... 39

LIST OF SYMBOLS..... 49

FIGURES

1. Typical Arrangement of a Michelson Interferometer to Measure Length Changes..... 8

2. Relative Signal Strengths of V and V cos $\omega_m t$ at Twice the Modulation Frequency..... 17

3. Experimental Test Setup to Measure Γ..... 19

4. Measured J_o Versus PZT Volts P-P..... 20

5. PZT Volts Versus Γ..... 21

6. Experimental Scheme to Measure Γ with the PZT at 45 deg to the Beam..... 23

7. Signal Processing for a Modulated Interferometer..... 26

8. Fringe Counting and Interpolation..... 27

9. Experimental Test Setup To Find Interferometer System Resolution..... 30

10. Volts Applied to PZT Versus Fringe Change..... 31

11. Linear Frequency Response = 0 to 37 kHz at ±3 dB of System..... 32

12. Quartz Tube Test..... 34

TABLES

1. Piezoelectric Transducer at 90 deg..... 22

2. Piezoelectric Transducer at 45 deg..... 24

I. INTRODUCTION

Analysis of optical interference is a major task in such diverse fields as astronomy, metrology, vibration analysis, microscopy, shock- and gravity-wave research, optical fabrication, communications, and dimensional stability of materials, components, and structures. Demands for improved resolution (e.g., $<\lambda/1000$), reliability, and versatility require signal-analysis systems incorporating simultaneous real-time automated data output in digital and/or analog form, computer interfaces, bidirectional counting, fringe interpolation, fast response, and long-term stability in terms of insensitivity to changes in optical alignments or transmission characteristics. In this report, we describe a system suitable for the continuous measurement of a Michelson interference pattern.

A major application of this system is automatic tracking of the thermal expansion of composite materials over a wide temperature range. The system is also capable of linearly detecting acoustic emission bursts produced by microcracking in temperature-cycled composites. (This is because the interferometer responds to rapid changes of the sample ends or attached mirrors and exterior noise that is not related to the change of the sample is damped out.)

The basic approach includes the phase modulation of a Michelson interferometer fringe pattern, and then the comparison of the processed laser signal with a reference frequency. The total phase change between these two signals is converted to a voltage that is proportional to the change in optical path length difference of the interferometer. The signal processing is partly a homodyne technique as opposed to the generally more complex heterodyne methods.[1,2] It has been recognized that phase modulation is one of the best approaches to automatic and directional fringe counting.[3] The directional motion can be found from the integrated intensity as received by a single photodetector. Detection of poor-quality (low-visibility) fringes is also possible, with no dependence on polarization states. The basic approach for a system using phase modulation in one arm of a Michelson interferometer

was outlined in Reference 4. Theory for the detailed analysis of another such system, as well as its general implementation and calibration, is described in Section II.

II. THEORY

A. MICHELSON INTERFEROMETER

In a Michelson interferometer, a coherent light beam is split and recombined. For our purposes, a helium-neon (HeNe) laser is used as a source, and a silicon photodetector is used as a receiver (Fig. 1). The two beams have traversed different paths and can be designated as follows (z is the direction of propagation), assuming plane polarization:

$$E_1 = A_1(x,y)\exp\{i[\omega t - 2kz_1 + \phi_1(x,y)]\} \tag{1a}$$

$$E_2 = A_2(x,y)\exp\{i[\omega t - 2kz_2 + \phi_2(x,y)]\} \tag{1b}$$

where A is real. The total field is the sum of these amplitudes, $E = E_1 + E_2$, and the intensity is proportional to the square of the field or

$$I = \frac{1}{2}\varepsilon_o c\, EE^* \tag{2}$$

$$I(x,y) = \frac{1}{2}\varepsilon_o c\{A_1^2(x,y) + A_2^2(x,y) + 2A_1(x,y)A_2(x,y)\cos$$

$$[2k(z_2 - z_1) + \phi_1(x,y) - \phi_2(x,y)]\}$$

The detector converts the total power received to a current and, hence, a voltage. The total power is found by integrating the intensity, Eq. (2), over the detector area (the entire beam). The resultant voltage is therefore[4,6]

$$V = V_o\{\ell + \beta\cos[2k(z_2 - z_1) + \phi_o]\} \tag{3}$$

where β is between 0 and 1. Henceforth, since we are making difference measurements, ϕ_o will be neglected so that

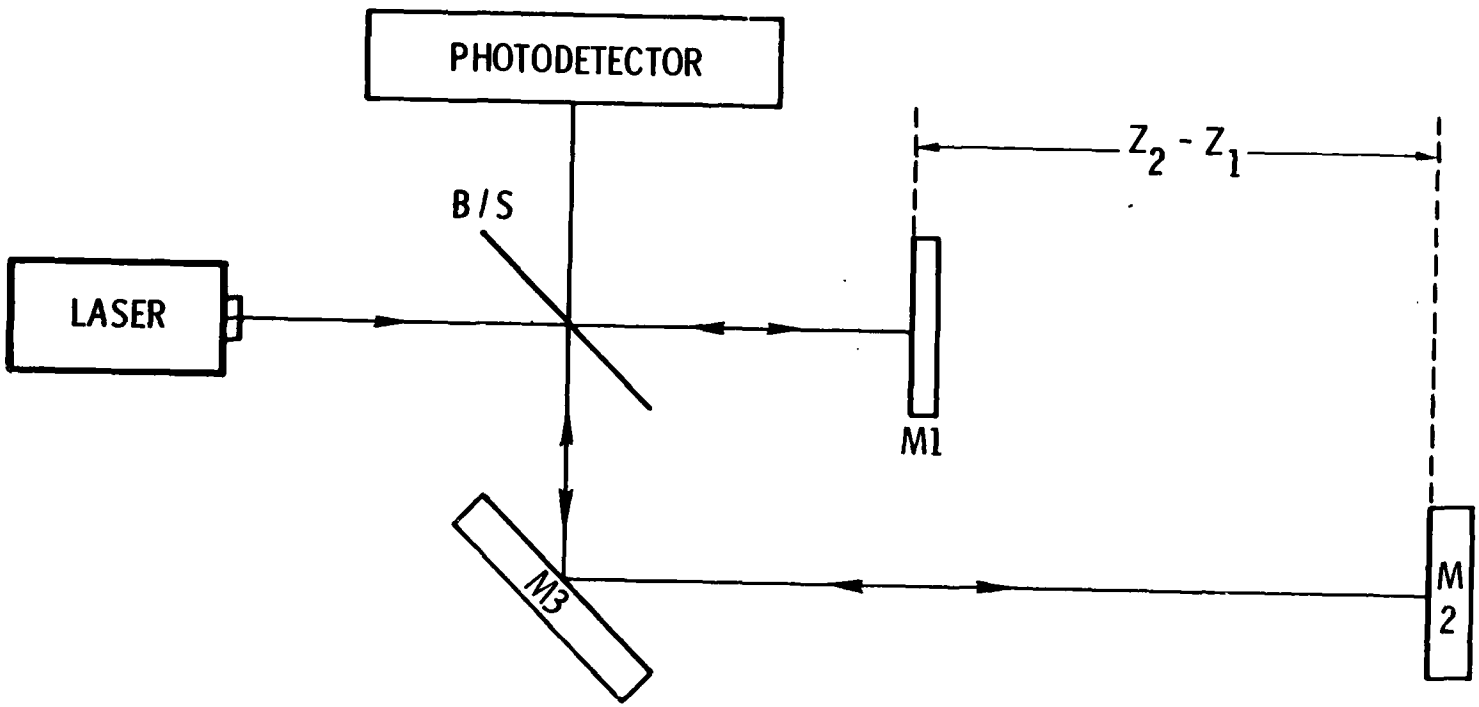

Fig. 1. Typical Arrangement of a Michelson Interferometer to Measure Length Changes

$$\phi = 2k(z_2 - z_1) = \frac{4\pi n}{\lambda}(z_2 - z_1)$$

Further, call $\ell = z_2 - z_1$ so that

$$\phi = \frac{4\pi n}{\lambda}\ell \tag{4}$$

and

$$V = V_o(\ell + \beta \cos \phi) \tag{5}$$

V_o is a function of the laser power, optical losses, detector responsivity, and the resistor used in the current to voltage conversion. β is a function of the relative beam strengths, relative wavefront distortions, and beam alignment. Also, ϕ_o is a function of the relative wavefronts.

The objective is to develop a signal-processing scheme that can conveniently measure the changes in ϕ and still be insensitive to changes in V_o and β. As mentioned, the approach taken is to modulate ϕ so that $\phi \rightarrow \phi + \Gamma \sin \omega_m t$. Here, Γ is the depth of modulation. Equation (5) becomes[4]

$$V = V_o [\ell + \beta \cos(\phi + \Gamma \sin \omega_m t)] \tag{6}$$

if $\omega_m \ll \omega$. Equation (6) can be expanded in a Fourier-Bessel series.

$$V = V_o\{1 - \beta J_o(\Gamma) \cos \phi \; 2\beta \sum_{n=0}^{\infty} [J_{2n}(\Gamma) \cos \phi \cos 2n \omega_m t - J_{2n+1}(\Gamma) \sin \phi \sin(2n + 1)\omega_m t]\} \tag{7}$$

B. MODULATION METHODS

The phase, ϕ, or $2k\ell$, can be altered by changing k or ℓ, the geometrical path. The approach used here involves varying ℓ with a piezoelectrically driven mirror, M_3, within the interferometer (Fig. 1). In this case,

$$\Gamma = 2k\,\Delta\ell_{max} \tag{8}$$

Another approach would be to insert an electro-optic modulator in one of the interferometer's beams. This device is a crystal whose index of refraction is controlled by an applied voltage. Here, k is altered over a portion of one of the beams. In this instance,

$$\Gamma = 2\ell_c\,\Delta k_{max} \tag{9}$$

and

$$\Delta k = \frac{k_o n_o^2}{2} r_{63} \Xi_z$$

Yet another approach incorporates a frequency-modulated laser. For low frequencies,

$$\Gamma = \frac{2\,\ell\Delta\omega_{max}}{c} \tag{10}$$

where $\Delta\omega_{max}$ is the peak frequency deviation.

Still another approach involves phase modulating the laser source outside the cavity with an electro-optic crystal. Here, the electric-field input to the interferometer is denoted (suppressing spatial dependence).

$$E = E_o \sin(\omega t + \gamma \cos \omega_m t)$$

where γ is the modulation index of the carrier. The intensity output of the interferometer will then be

$$I = \frac{I_o}{2}\left\{1 + \cos\left[\phi - 2\gamma \sin\frac{\omega_m \ell}{c} \sin\left(\omega_m t - \frac{\omega_m \ell}{c}\right)\right]\right\}$$

For small ω_m, i.e., $\omega_m < c/\ell$, this reduces to Eq. (6) with

$$\Gamma = \frac{-2\gamma\omega_m \ell}{c} \tag{11}$$

Finally, the modulation technique used by Hewlett-Packard in their commercial interferometer is somewhat different. Instead of a sinusoidal phase modulation, a linear modulation is produced. This results in an interferometer output

$$V = V_o[1 + \beta \cos(\phi + \omega_m t)]$$

This type of signal is in a convenient form for signal processing, and such processing is insensitive to βV_o, the amplitude of the alternating current (ac) signal. This is just the form sought by electronic manipulation of signals of the form given in Eq. (6). This manipulation is detailed in Section III.

III. ANALYSIS

A. SIGNAL PROCESSING

Equation (7) describes the signal received from the Michelson interferometer. The main objective is to construct from this an ac signal whose phase varies precisely as the static phase difference, ϕ, of the interferometer. This electrical signal can be combined with a reference signal in a phasemeter and/or an A minus B (A-B) counter. (If the results of two interferometers were to be compared, a reference signal would not be required.) A phasemeter measures ϕ directly, and the A-B counter directionally records phase changes of 2π.

The formation of such an ac signal is accomplished by multiplying (mixing) V, Eq. (6) or (7), by $1 + \cos \omega_m t$. This can also be viewed as mixing V with $\cos \omega_m t$ and adding this result to V. Define then V_s as

$$V_s = (1 + \cos \omega_m t)V \tag{12}$$

write $\omega = \omega_m$, and note that

$$\cos \omega t \cos 2n\omega t = \frac{1}{2} \cos(2n - 1)\omega t + \frac{1}{2} \cos(2n + 1)\omega t$$

$$\cos \omega t \sin(2n + 1)\omega t = \frac{1}{2} \sin 2n\omega t + \frac{1}{2} \sin(2n + 2)\omega t$$

Then

$$V \cos \omega t = V_o \cos \omega t$$

$$+ \beta V_o \left[-J_o \cos \phi \cos \omega t + \sum_{n=0}^{\infty} J_{2n} \cos \phi \cos(2n - 1)\omega t \right.$$

$$+ \sum_{n=0}^{\infty} J_{2n} \cos \phi \cos(2n + 1)\omega t - \sum_{n=0}^{\infty} J_{2n+1} \sin \phi \sin 2n\omega t$$

$$- \sum_{n=0}^{\infty} J_{2n+1} \sin \phi(2n + 2)\omega t]$$

In the first sum, $n = m + 1$. It then becomes

$$\sum_{m=-1}^{\infty} J_{2m+2} \cos \phi \cos(2m + 1)\omega t = J_o \cos \phi \cos \omega t$$

$$+ \sum_{n=0}^{\infty} J_{2n+2} \cos \phi \cos(2n + 1)\omega t$$

In the fourth sum, $n = m - 1$. It becomes

$$- \sum_{m=1}^{\infty} J_{2m-1} \sin \phi \sin 2m\omega t$$

Note that this sum can start at $m = 0$ since $\sin 0 = 0$.

Combining all the terms,

$$V \cos \omega t = V_o \cos \omega t + \beta V_o \sum_{n=0}^{\infty} (J_{2n+2} + J_{2n}) \cos \phi \cos(2n + 1)\omega t$$

$$-(J_{2n+1} + J_{2n-1}) \sin \phi \sin 2n\omega t$$

But since

$$J_{n-1}(\Gamma) + J_{n+1}(\Gamma) = \frac{2n}{\Gamma} J_n(\Gamma)$$

then

$$J_{2n}(\Gamma) + J_{2n+2}(\Gamma) = \frac{2}{\Gamma}(2n + 1)J_{2n+1}(\Gamma)$$

and

$$J_{2n-1}(\Gamma) + J_{2n+1}(\Gamma) = \frac{2}{\Gamma}(2n)J_{2n}(\Gamma)$$

so that

$$V \cos \omega t = V_o \cos \omega t + \frac{2\beta V_o}{\Gamma} \sum_{n=0}^{\infty} \left[(2n + 1)J_{2n+1} \cos \phi \cos(2n + 1)\omega t - 2nJ_{2n} \sin \phi \sin 2n\omega t\right] \quad (13)$$

We now add Eqs. (7) and (13) to provide V_s according to Eq. (12).

$$V_s = V_o(1 + \cos \omega t) - \beta V_o J_o \cos \phi + 2\beta V_o \sum_{n=0}^{\infty} \{J_{2n+1}(\Gamma)[\frac{2n + 1}{\Gamma} \cos \phi \cos(2n + 1)\omega t - \sin \phi \sin(2n + 1)\omega t] + J_{2n}(\Gamma)[\cos \phi \cos 2n\omega t - \frac{2n}{\Gamma} \sin \phi \sin 2n\omega t]\} \quad (14)$$

With proper filtering and choice of Γ, this will yield the desired result, as can be seen using trigonometric identity, cos A cos B - sin A sin B = cos (A + B). In general, note that for the mth harmonic, if Γ = m and if all other harmonics are suppressed,

$$V_s = 2\beta V_o J_m(m) \cos(m\omega t + \varphi) \qquad (15)$$

This is true except for m = 1. In this case,

$$V_s = V_o \cos \omega t + 2\beta V_o J_1(1) \cos(\omega t + \phi)$$

This signal can be used if the direct current (dc) term, V_o, in the original signal, Eq. (6), is nullified or otherwise compensated. For a complete ac system, we choose the next lowest term, m = 2. Figure 2 shows the signal strengths of V and V cos $\omega_m t$ at twice the modulation frequency, m = 2. Now we have an ac signal whose phase is equal to the phase of the interferometer. The amplitude, βV_o, does not affect a zero-crossing-type phase measurement. Therefore, the measurement capability is highly insensitive to changes in laser power, optical losses, relative beam strengths, and beam alignment. This results in a highly reliable instrument.

B. MEASUREMENT OF DEPTH OF MODULATION

In arriving at our results, Eq. (15), it was necessary to set $\Gamma = m(2)$ and suppress all other terms. Filtering the other signal components will be discussed in Section IV.C. Determining the depth of modulation, Γ, is the concern here. Note, however, that it is not strictly necessary to set $\Gamma = 2$. It can actually be different (Fig. 2), while achieving "balance" electronically. However, it is advantageous to be able to measure Γ.

This is done by measuring the as-received dc voltage with and without modulation. The voltage without modulation, V_n, we get from Eq. (5)

$$V_n = V_o (1 + \beta \cos \phi)$$

and the dc voltage with modulation V_m, we get from Eq. (7).

$$V_m = V_o[1 + \beta J_o (\Gamma) \cos \phi]$$

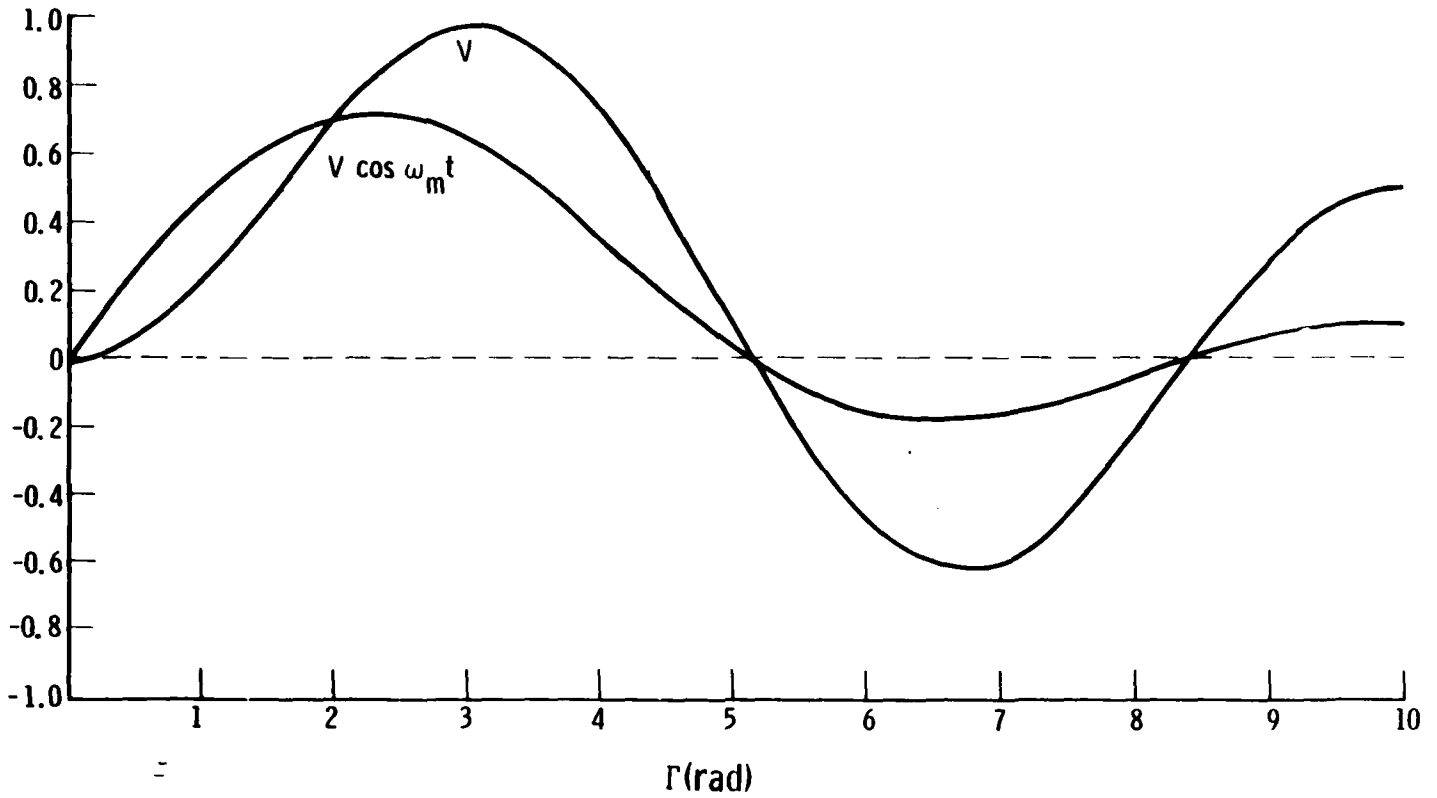

Fig. 2. Relative Signal Strengths of V and V cos $\omega_m t$ at Twice the Modulation Frequency

V_o must also be measured, in which case we compute $J_o(\Gamma)$ from

$$J_o(\Gamma) = \frac{V_m - V_o}{V_n - V_o} \tag{16}$$

Figure 3 shows an experimental approach to the measurement of Γ. Adjusting the 20-V supply moves one arm of the interferometer and permits a measurement of V_o. When the switch, S_1, is closed, V_m is measured. When S_1 is open, V_n is measured. The fraction, Eq. (16), is plotted in Fig. 4 for various modulation amplitudes. Using known values of $J_o(\Gamma)$,Γ versus applied piezoelectric transducer (PZT) voltage is shown in Fig. 5, which shows the expected linear dependence. This process is evaluated in Table 1.

Figure 6 shows a setup for measuring the same thing (Table 2) but with a different optical geometry closer to the one actually used. One would expect a factor of $(2)^{1/2}$ increase in the sensitivity to applied voltage, although this was not observed. It may be that besides modulating the path, l, as in Eq. (8), either or both beam alignment and wavefront character are also being modulated, invalidating that equation.

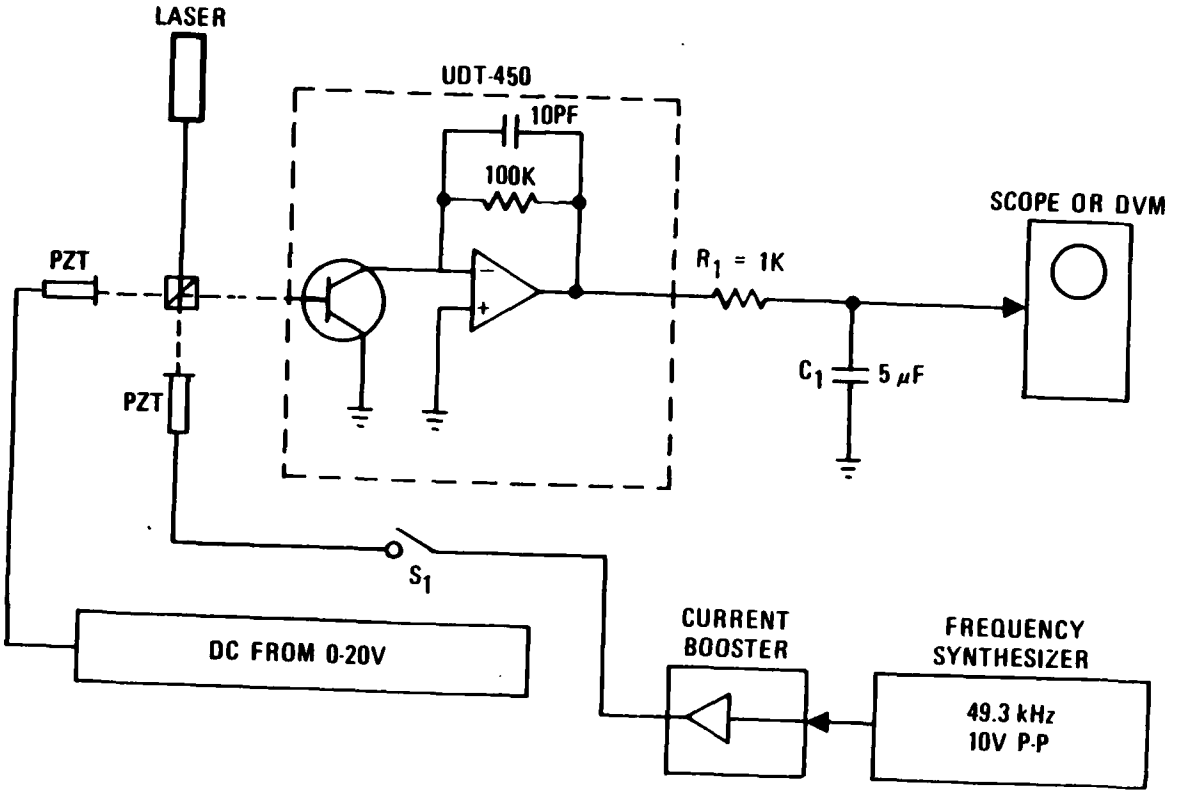

Fig. 3. Experimental Test Setup to Measure F

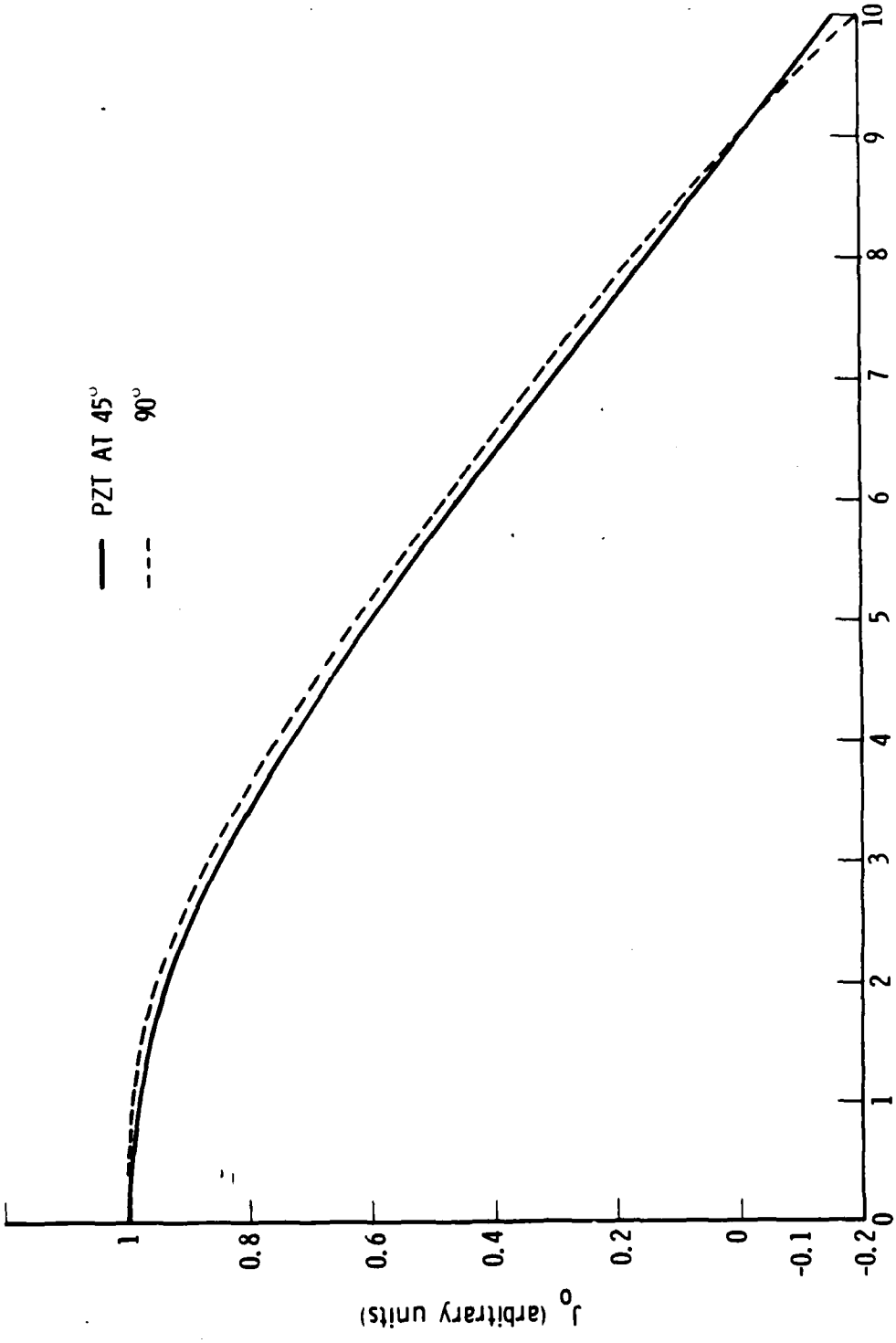

Fig. 4. Measured J_o Versus PZT Volts P-P

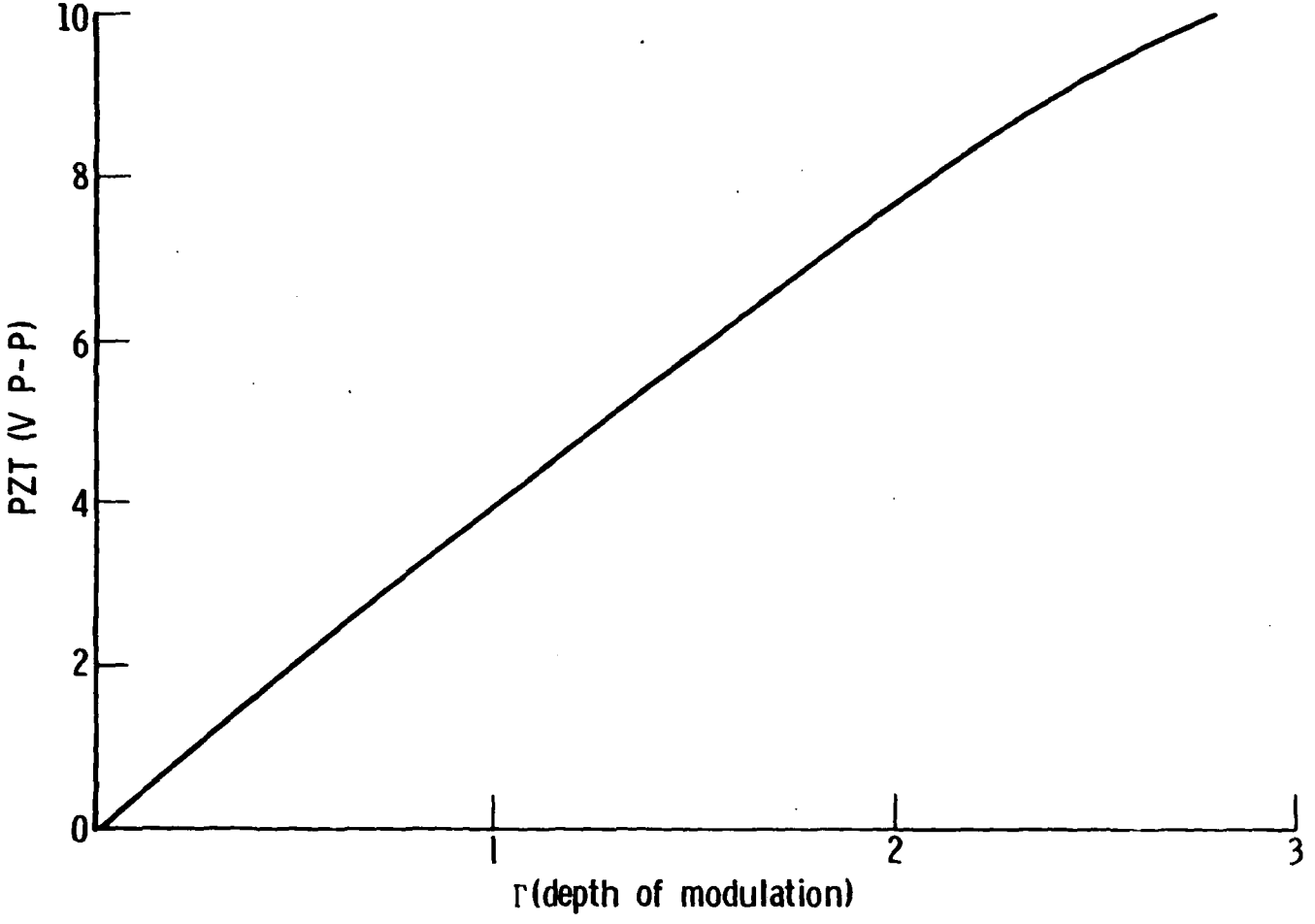

Fig. 5. PZT Volts Versus Γ

Table 1. Piezoelectric Transducer at 90 deg

$V_m - V_o$ (V)	$V_n - V_o$ (V)	VP-P to PZT	J_o (Γ)	Γ
0.76	4.12	10	-0.184	2.80
0.19	4.12	9	-0.0461	2.50
0.57	4.12	8	0.138	2.13
1.29	4.12	7	0.313	1.80
1.99	4.12	6	0.483	1.50
2.61	4.12	5	0.633	1.28
3.16	4.12	4	0.767	1.00
3.58	4.12	3	0.869	0.70
3.09	4.12	2	0.947	0.48
4.07	4.12	1	0.988	0.20
4.12	4.12	0	1.00	0

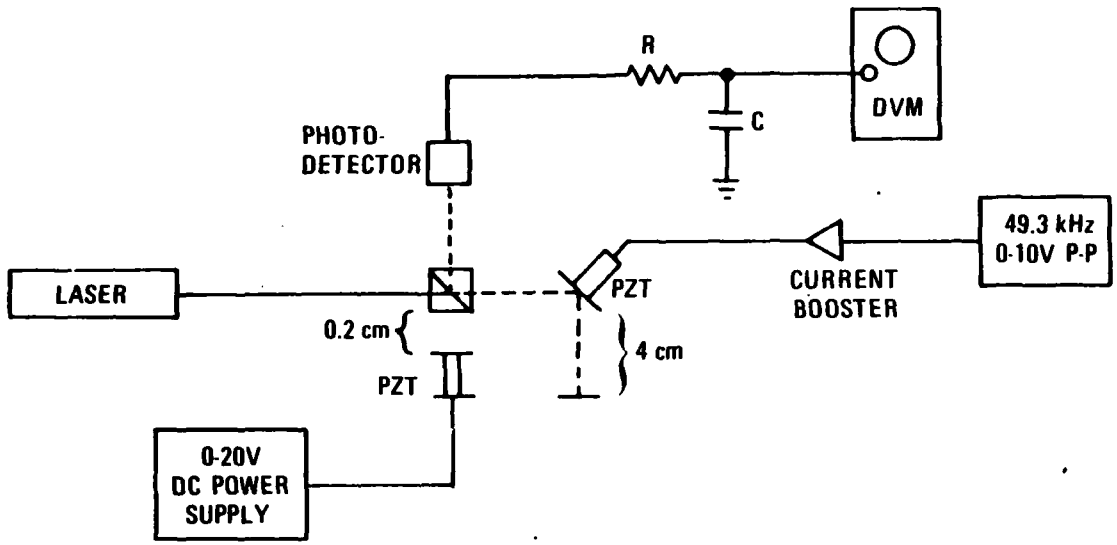

Fig. 6. Experimental Scheme to Measure Γ with the PZT at 45 deg to the Beam

Table 2. Piezoelectric Transducer at 45 deg

$V_{m_{(V)}} - V_o$	$V_{n_{(V)}} - V_o$	VP-P to PZT	J_o (Γ)	Γ
500 m	3.14	10	-0.159	2.74
50 m	3.14	9	0.0159	2.40
480 m	3.14	8	0.153	2.13
980 m	3.14	7	0.312	1.83
1.46	3.14	6	0.465	1.60
1.93	3.14	5	0.615	1.30
2.30	3.14	4	0.732	1.10
2.68	3.14	3	0.854	0.75
2.92	3.14	2	0.930	0.55
3.07	3.14	1	0.978	0.30
3.14	3.14	0	1.00	0.00

IV. DESIGN

A. CIRCUITRY

Figure 7 shows the circuitry that performs the mathematical operations indicated. Note that in generating V_s, Eq. (12), we multiply V by cos $\omega_m t$, which is shifted in phase by 90 deg from the original phase-modulated interferometer, Eq. (6). This phase shift occurs naturally within the PZT, so the electronics are simplified. The PZT may be viewed as a damped oscillator driven at resonance (~50 kHz). Therefore, the applied force (voltage) is 90 deg out of phase with the displacement. Call the driving voltage cos $\omega_m t$, then the actual displacement will be proportional to sin $\omega_m t$. This is consistent with the analysis given. Therefore, the signal driving the PZT, cos $\omega_m t$, is mixed with V by the multiplier as specified. The output of the multiplier, V cos $\omega_m t$, is summed with V to provide V_s. The filter network conditions V_s (Section IV.C), and then it is digitized by the clippers as is the frequency-doubled reference. The up-down counter does not work reliably for synchronous reception of these two signals, so a coincident avoid network is used to filter such pulses. The counter and digital-to-analog converter provide a continuous voltage proportional to phase changes (length changes) in the interferometer. Their operation is detailed in Section IV.B.

B. FRINGE COUNTING AND PHASE INTERPOLATION

The process of phase interpolation is accomplished by using an up-down counter and a digital-to-analog converter. The up-down counter is a device that will count up for pulses on one input and down for those on the other and store the count value in a binary code. The digital-to-analog converter is a circuit composed of ratioed quantities of resistances in series and parallel to produce a voltage step value proportional to the input binary code information. The reference and processed interferometer signals are applied to the up and down inputs of the counter. One fringe shift (2π phase shift) results in one count and one unit of voltage increase at the digital-to-analog converter output (Fig. 8). Intermediate phase values result in a digital-to-analog converter output of a unit squarewave whose duty cycle equals the phase

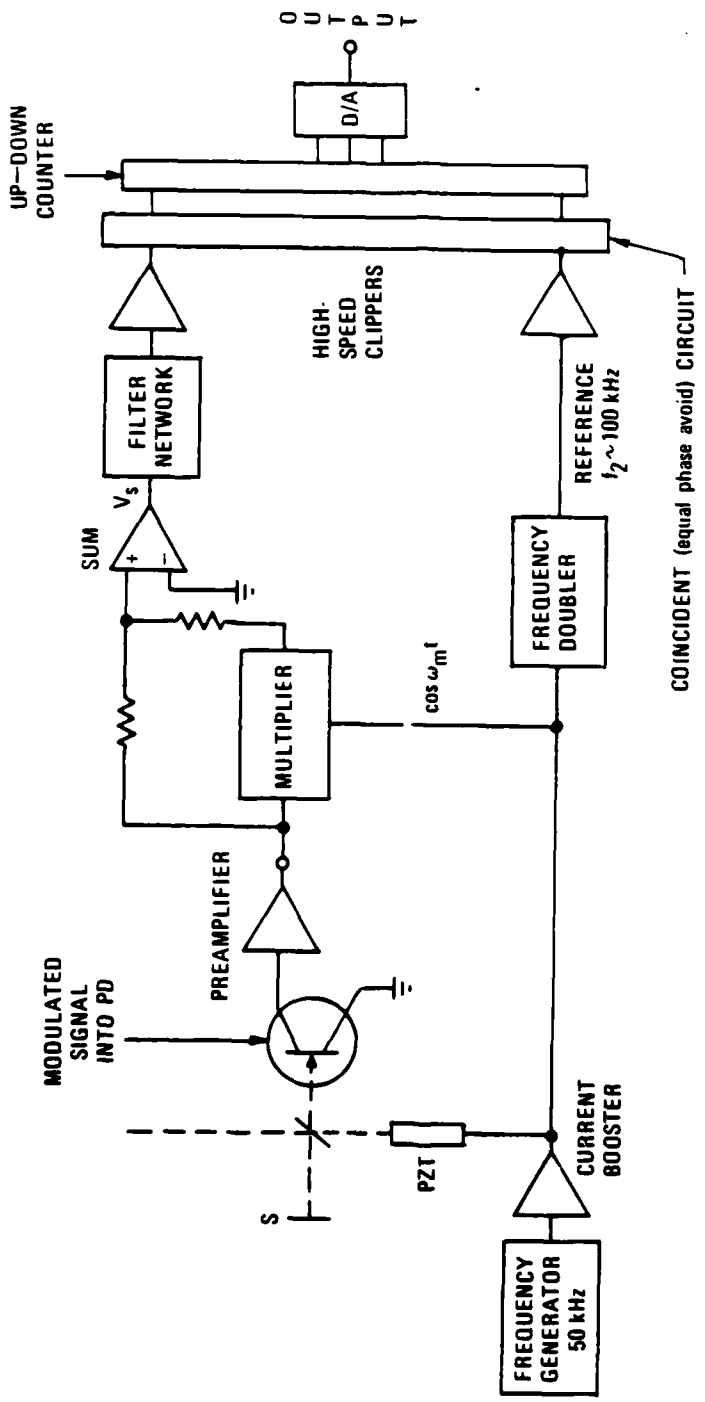

Fig. 7. Signal Processing for a Modulated Interferometer

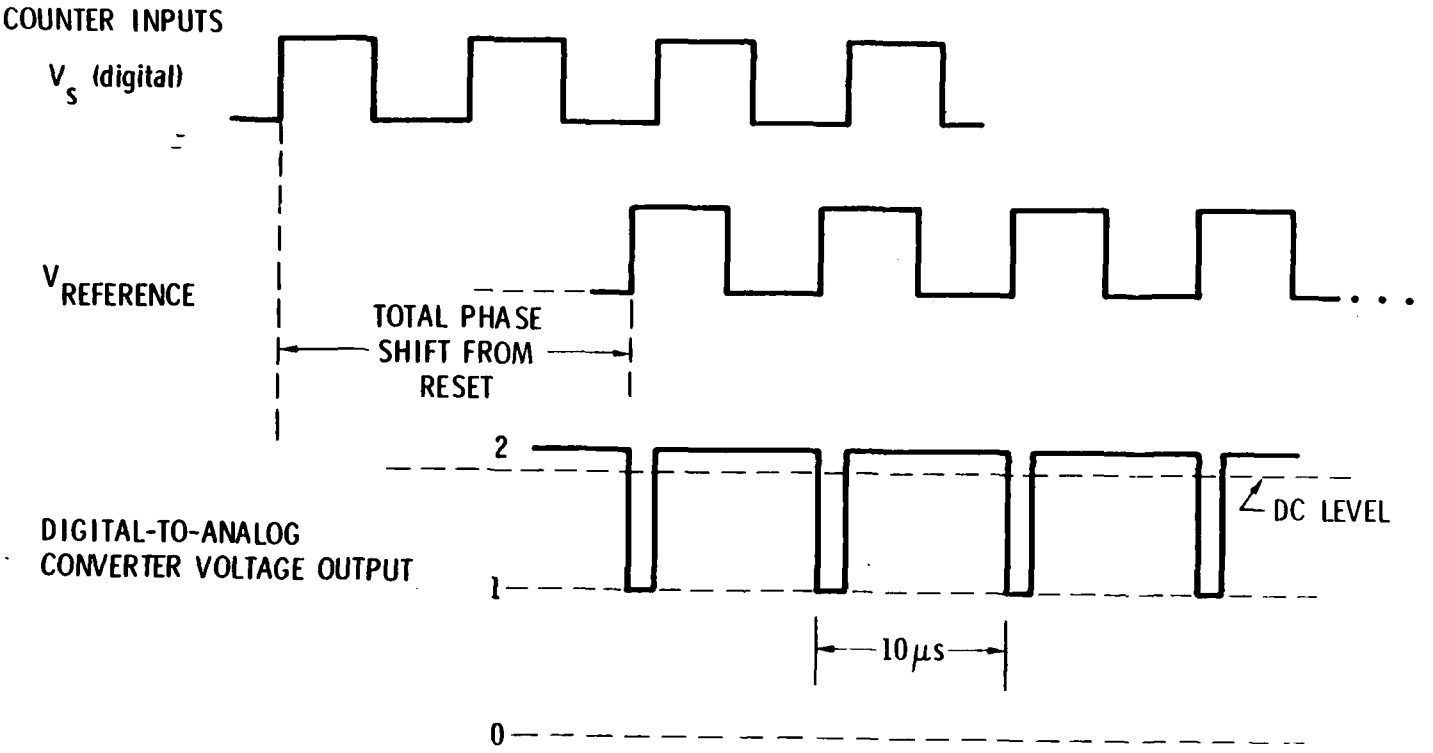

Fig. 8. Fringe Counting and Interpolation

angle. Therefore, the direct current digital-to-analog output is a continuous voltage proportional to the total phase change of the interferometer from some reset condition.

C. DISTORTION ANALYSIS

The choice of filter network (Fig. 7) determines the characteristics of the device. With a high-Q bandpass function at $2\omega_m$, Eq. (15) is easily resolved from Eq. (14). However, this increases the response time. If the filter is widened, the system is faster, but then different harmonics are passed. The inclusion of different harmonics produces nonlinearities in the interpolation technique and can even cause incorrect counting. Miscounting results when the amplitude of one of the harmonics is greater than the $2\omega_m$ term.

For $\Gamma = 2$, $\beta = 1$ and $\omega_m/2\pi = 50$ kHz, the relative maximum amplitudes are, from Eq. 14, at 50 kHz, 2.26; 100, 1; 150, 0.55; 200, 0.19; and 250, 0.05.

Reducing the 50-kHz signal by at least 40% is then essential to proper counting. The nonlinearities produced by harmonic distortions are considered by looking at one harmonic at a time. If we have a harmonic whose relative amplitude is ε, then the maximum displacement error will be $\varepsilon\lambda/4\pi = 2\ \mu\text{in.} \times \varepsilon$.

Another consideration is the effect of mirror velocity, V. The received frequency at 50 kHz is shifted by the amount $f = 2V/\lambda$, and the higher harmonics by nf. This is a factor only when designing a filter for extreme dynamic conditions. For thermal expansion measurement, e.g., a quartz tube 12 in. long cooled at 1 K/min, $f = 0.004$ Hz, which is entirely negligible.

The filter described in Section V is a fairly wide bandpass filter. Although not optimal, it provides very good linearity and dynamic response. For example, it easily and reliably responds to sudden, large impulses to the optics supports. A filter design for maximum linearity might include notch filters at 50 and 150 kHz and a low-pass filter to eliminate the higher harmonics.

V. PERFORMANCE

A. RESOLUTION

The final calibrated output can be checked with a PZT (Burleigh PZ40) in one arm of the interferometer to produce a motion of 0 to 1.5 μm, when 0 to 100 V is applied (Fig. 9). This PZT characteristic is rated linear to ±10%. It has a substantial hysteresis. The plotted curve of voltage applied to the PZT versus fringe change of the interferometer can then be used to assess nonlinearities over one fringe. From Fig. 10, this error is ±0.2 mV, and 1 fringe = $\lambda/2$ = 9.5 mV, so the error is $\pm\lambda/95$ = ±0.26 μin.

To improve this error, it is necessary to balance the signals at the summing amplifier (Fig. A-5, Appendix), and have the PZT resonate at exactly its resonant frequency. These adjustments are being incorporated into an improved version to give optimum performance of the unit. The large-scale linearity cannot be checked with the PZT. For the analog signal, it is just that of the digital-to-analog converter combined with the effect just discussed. The sensitivity is certainly greater than 0.26 μin.; it is about 3 μV/Å. The range of the interferometer is limited only by the coherence length of the beam and the number of counters in the signal processing system. With two counters, the range is at present ±128 counts, where 1 count = $\lambda/2$. For HeNe, this will be about ±40 μm or ±1500 μin.

B. FREQUENCY RESPONSE

Figure 11 shows the results of a test of the frequency response of the system after the inputs to the clippers (Fig. 7). A reference (100 kHz) signal was fed into one of the clippers. The other signal was modulated from 0 to 100 kHz using an HP Model 3325 A frequency synthesizer. The Y-scale is the attenuation of the sinusoidal output of the digital-to-analog converter as measured by the decibel conversion scale of a Nicolet 440 A spectrum analyzer. The graph shows that the digital section-analog output has a -3 dB point near 40 kHz, which is more than adequate. The frequency response of the overall

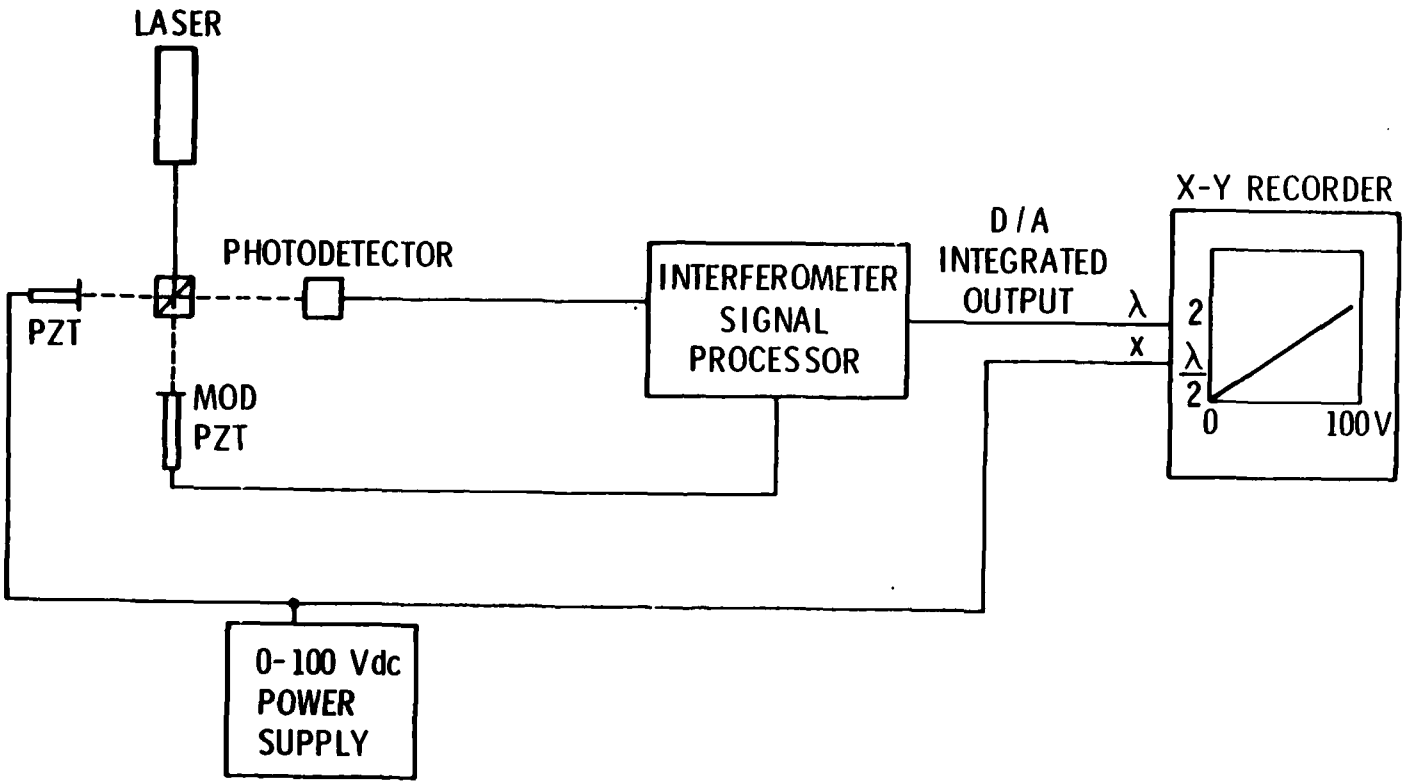

Fig. 9. Experimental Test Setup to Find Interferometer System Resolution

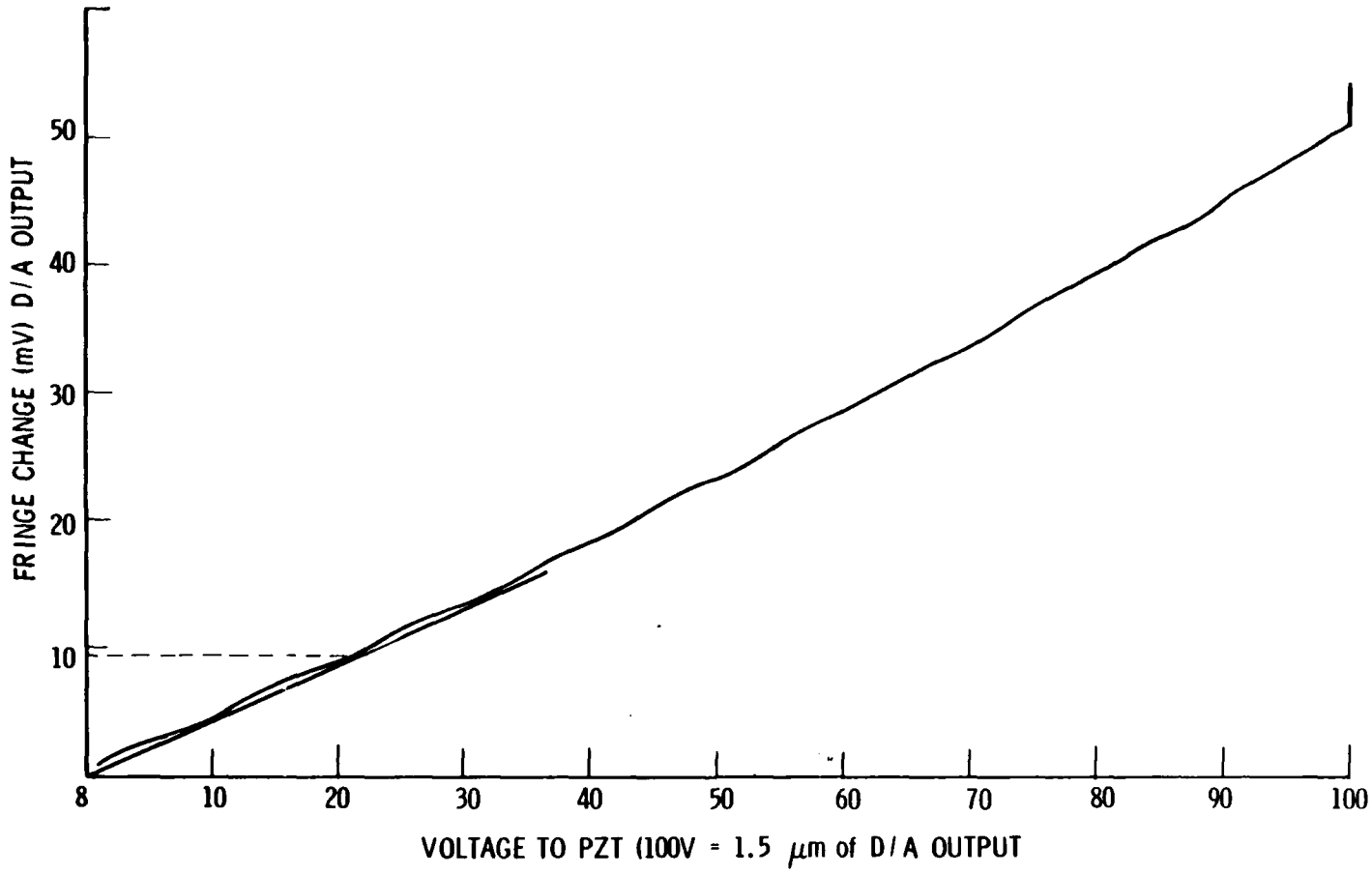

Fig. 10. Volts Applied to PZT Versus Fringe Change (1 Fringe = $\frac{\lambda}{2}$ = 10 mV)

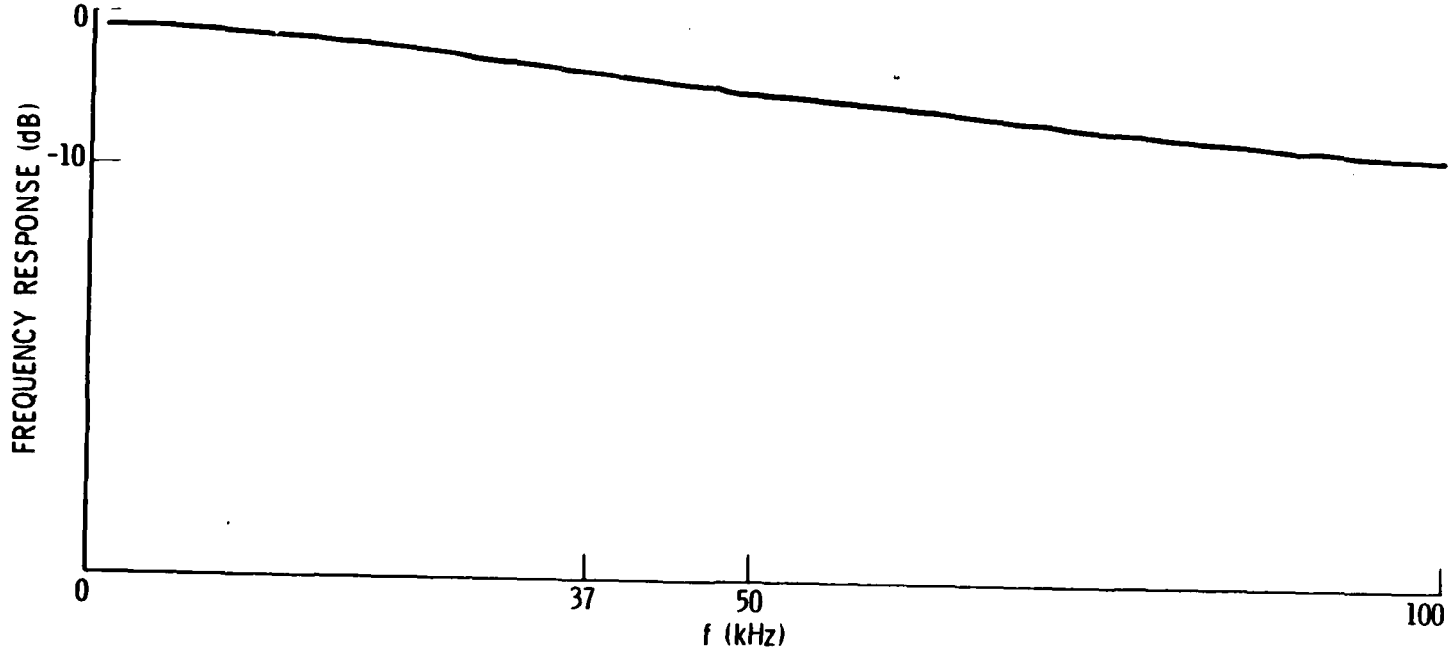

Fig. 11. Linear Frequency Response = 0 to 37 kHz at ±3 dB of System

system depends largely, therefore, on the filter network (Fig. 7). More elaborate testing would be required to measure the total response.

C. THERMAL EXPANSION TESTING

Figure 12 shows the results of a measurement of the thermal expansion of 12 long by 1/2-in.-diameter quartz tube. The PZT pusher providing the modulation frequency was situated at 45 deg next to a beam splitter in one arm of the interferometer so that closely parallel beams could be reflected to one end of the rod and to a mirror mounted at the other end (Fig. 1). The rod was in a vacuum; the beam splitter was a few centimeters from the window of the furnace. The curve is recorded in real time, corresponding to the 1 to 2°C/min heating-cooling rate. The small $\Delta L/L$ displacements on returning to the same temperature may be attributed to temperature gradients in the sample. The system output has been electronically adjusted with a voltage proportional to the sample length, so that $\Delta L/L$ (10^{-6}) or microstrain can be plotted on the X-Y recorder. The results are as expected for a quartz tube.[6]

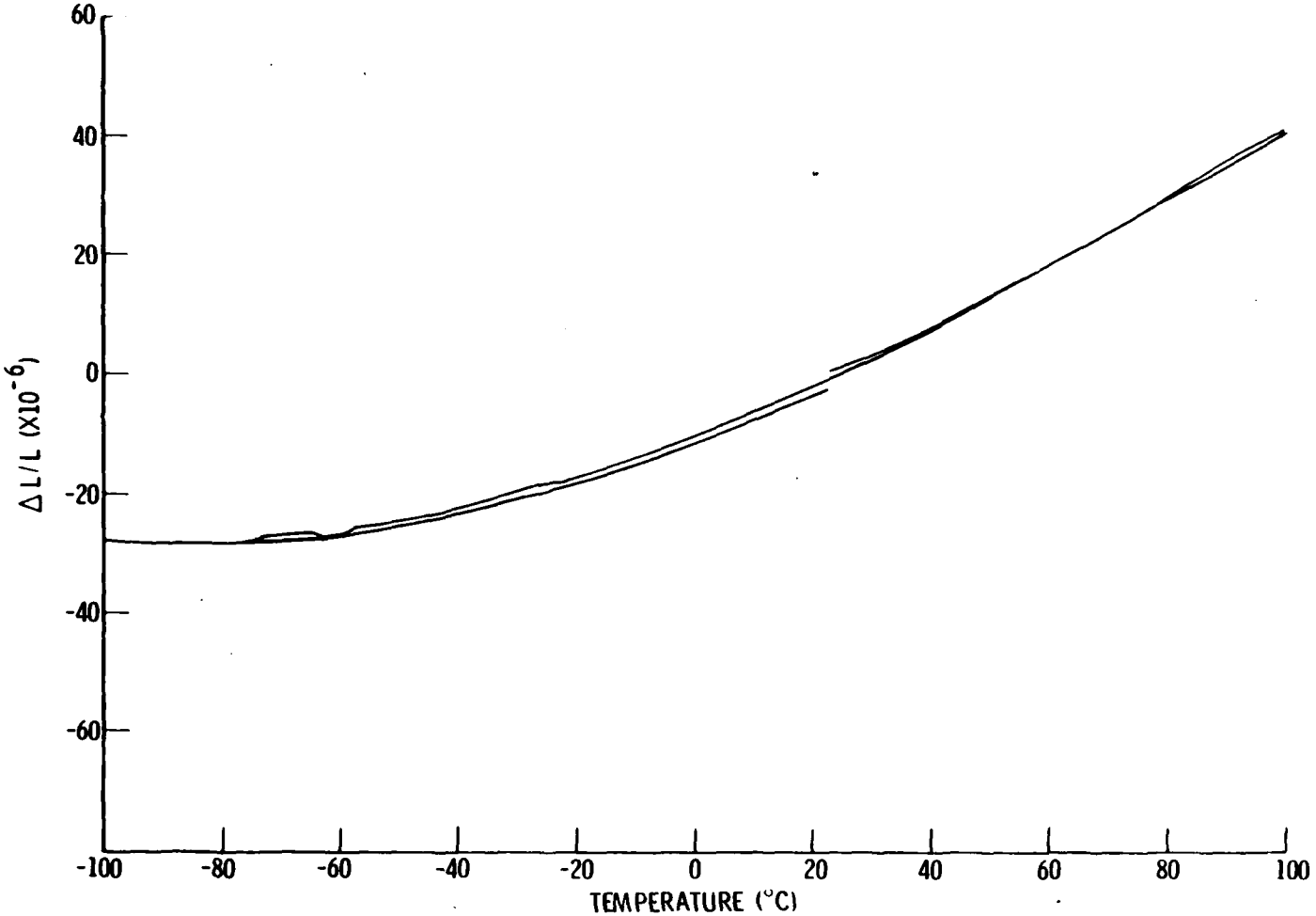

Fig. 12. Quartz Tube Test

VI. DISCUSSION

It has been found that the interferometer-signal-processing system is highly stable and linear to about ±60 Å. Further, because it is an ac system using FM-type detection, it meets the objective of being insensitive to signal changes brought on by changes in laser power, optical losses, relative beam strengths, and beam alignment. The required laser, optical components, and the electronic circuitry outlined are far less expensive than comparable commercial units. This unit, furthermore, is suitable for the detection of acoustic emission signals in the 0- to 30-kHz range.

REFERENCES

1. S. Sizgoric and A. A. Gundjian, "An Optical Homodyne Technique for Measurement and Amplitude and Phase of Subangstrom Ultrasonic Vibrations," Proc. IEEE, 1313-1314 (1969).

2. K. Tanaka and Y. Ohtsuka, "Laser Heterodyne Detection of Slowly Varying Displacements," J. Opt. 8 (1) 37-40 (1977).

3. S. H. Logue, Laser Interferometry Measuring System for Precision Gyro and Gas Bearing Parts, Final Report Contract NAS8-20568; Marshall Space Flight Center, Huntsville, Ala.; also, General Dynamics Report GDC-DBE-68-005 (5 December 1967).

4. S. A. Eselun and E. G. Wolff, "Advances in Interferometric Signal Analysis," ISA Trans. 19, (1) 59-64 (1980).

5. S. A. Eselun, H. D. Neubert, and E. G. Wolff, "Microcracking Effects on Dimensional Stability," Proceedings of 24th SAMPE Symposium, 1299-1309 (May 1979).

6. E. G. Wolff and S. A. Eselun, "Thermal Expansion of a Fused Quartz Tube in a Dimensional Stability Test Facility," Rev. Sci. Instr. 50 (4) 502-506 (1979).

APPENDIX

DETAILED CIRCUIT DIAGRAMS

A-1. Photodetector Amplifier (Board 1)

A-2. Photodetector Amplifier

A-3. Automatic Gain Control (Board 1)

A-4. 0.5-amp Current Booster

A-5. Multiplication and Summing Circuits (Board 2)

A-6. Coincident Avoid Counter (Board 3)

A-7. High-Pass Filter (Board 4)

A-8. High-Speed Clipper (Board 5)

A-9. Up-Down Counter, Analog Scale Set, Hexadecimal Display, and Digital-to-Analog Converter (Board 6)

BOARD No. 1

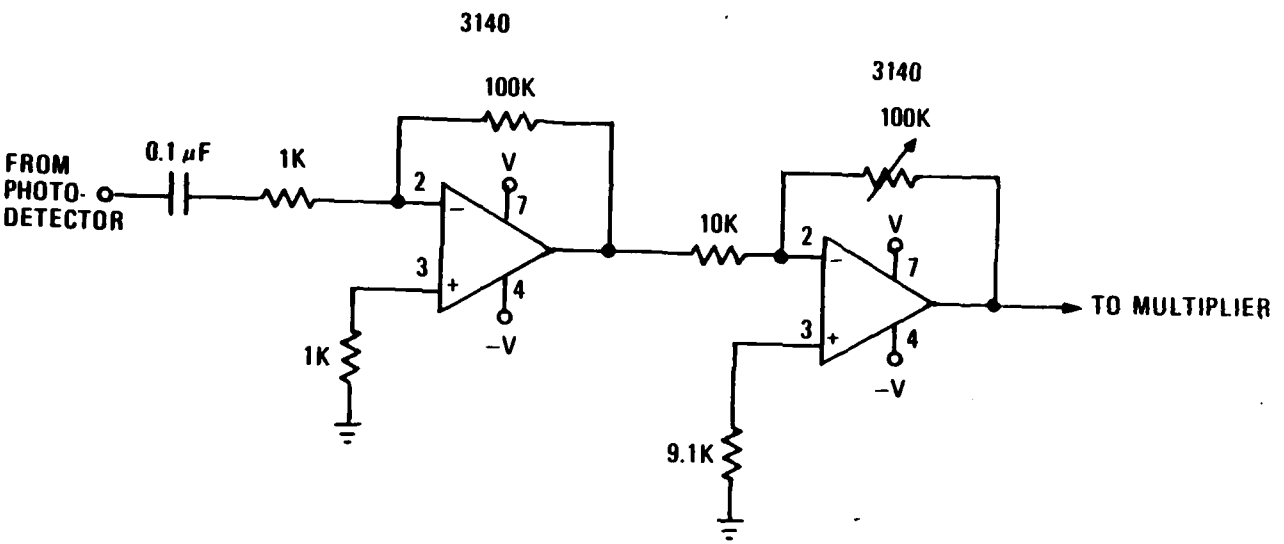

Fig. A-1. Photodetector Amplifier (Board 1)

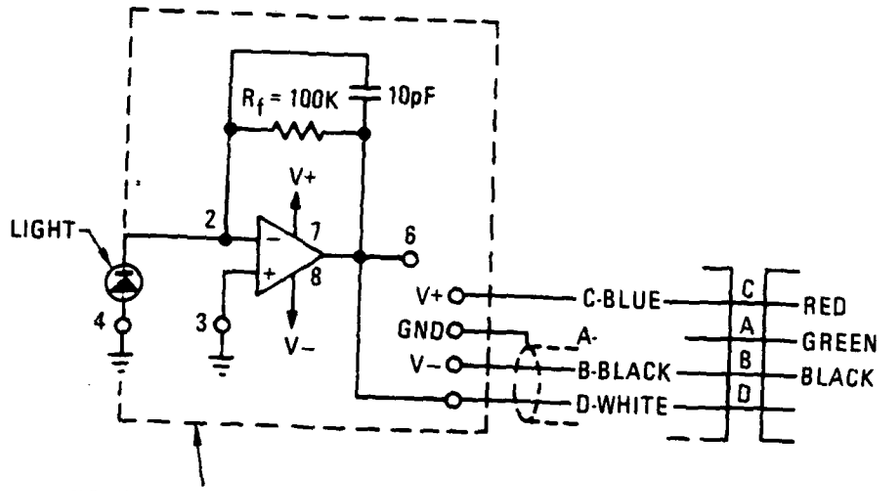

NOTES: Box chassis-length = 2¼ in.; width = 1 1/2 in.; depth = 1 3/8 in.
photodiode amplifier combination – UDT 450

Fig. A-2. Photodetector Amplifier

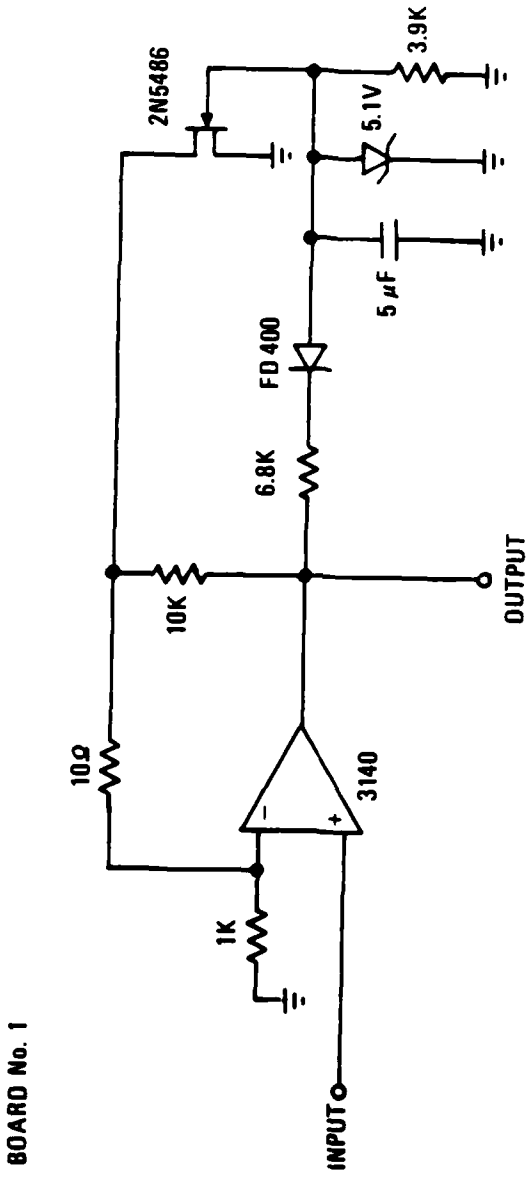

Fig. A-3. Automatic Gain Control

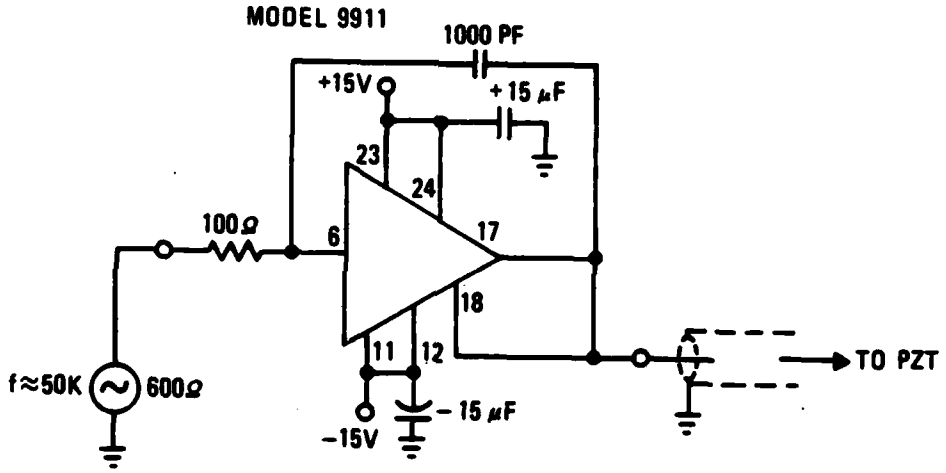

Fig. A-4. 0.5-amp Current Booster

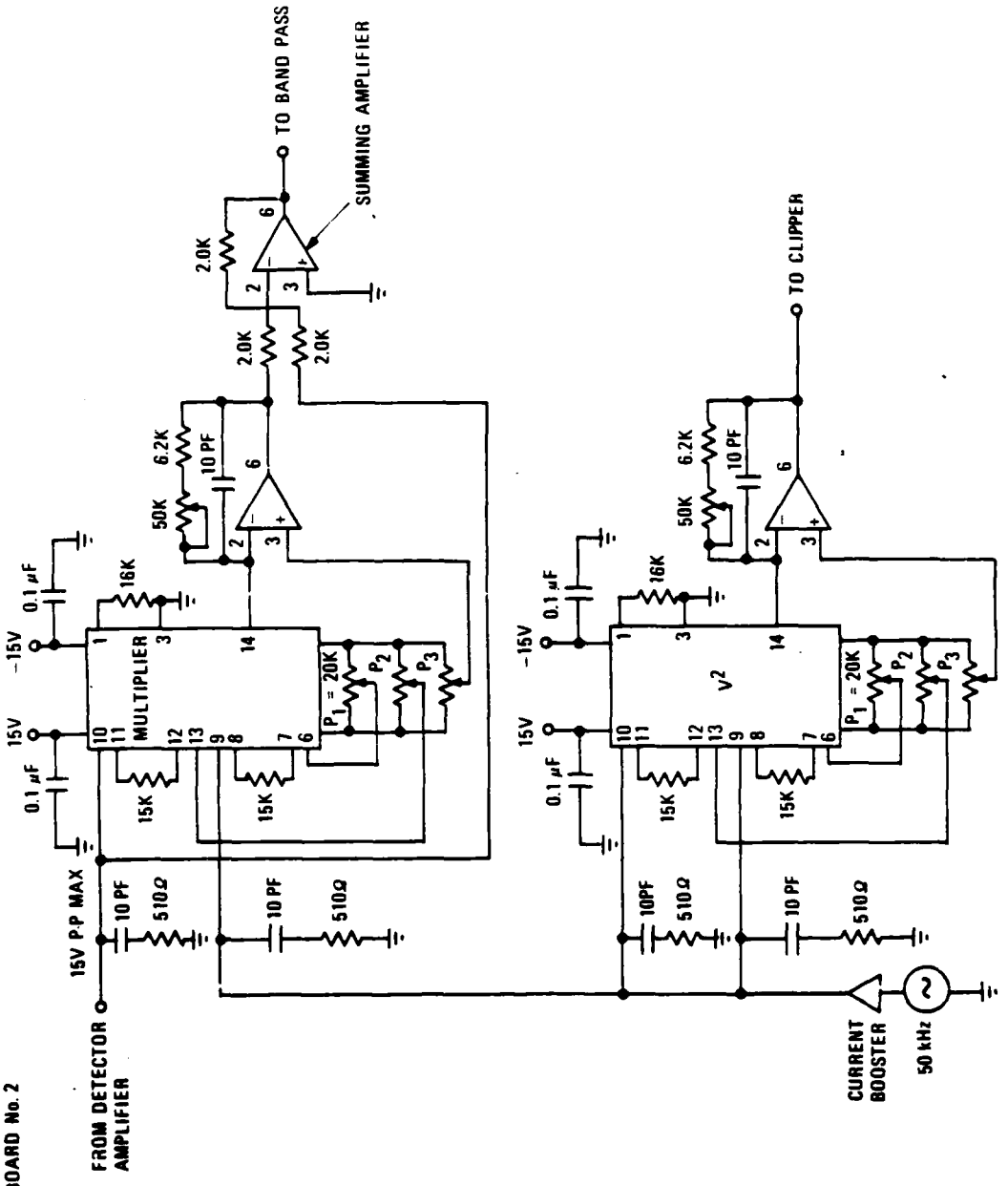

Fig. A-5. Multiplication and Summing Circuits

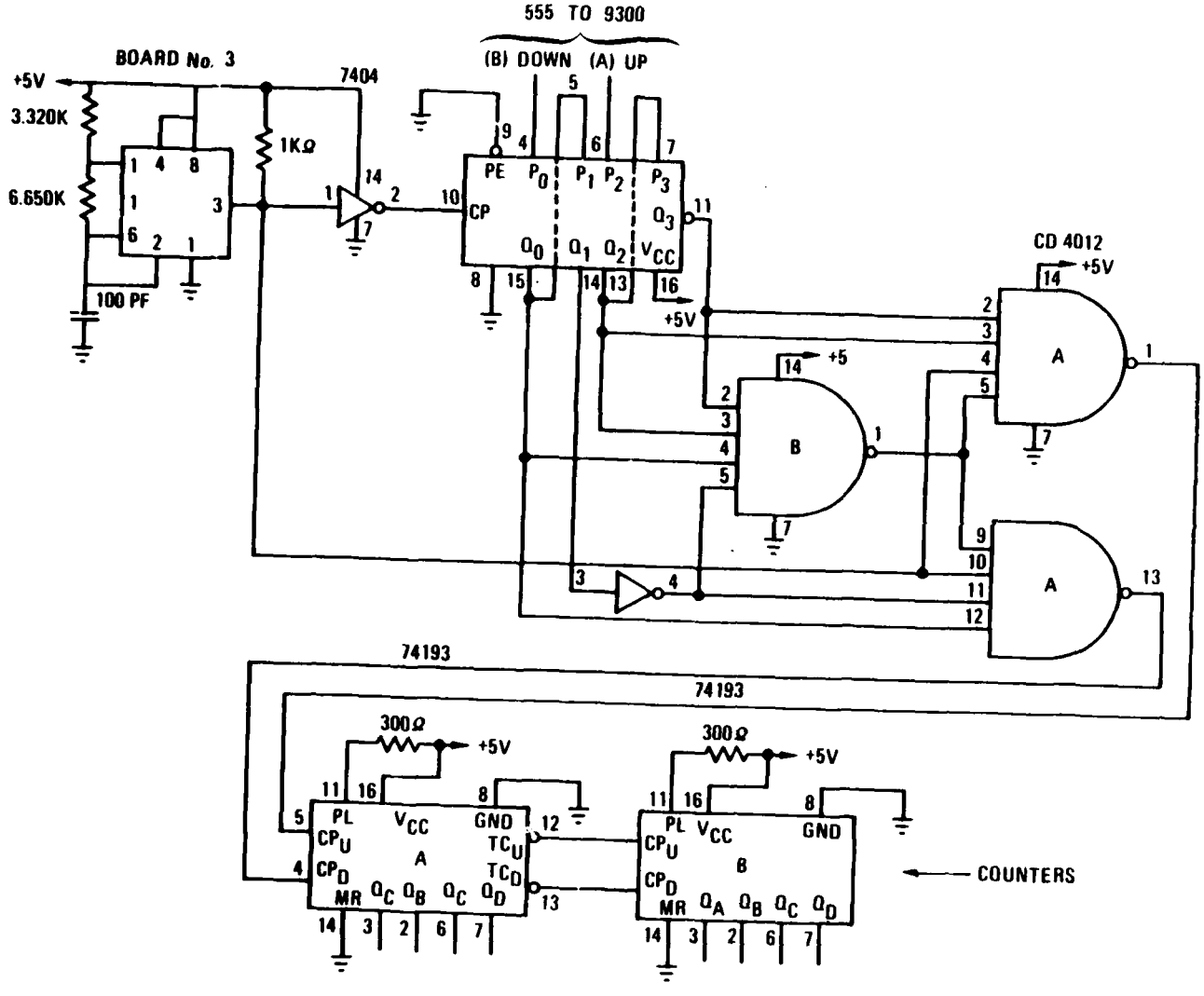

Fig. A-6. Coincident Avoid Counter (Up-Down)

BOARD No. 4

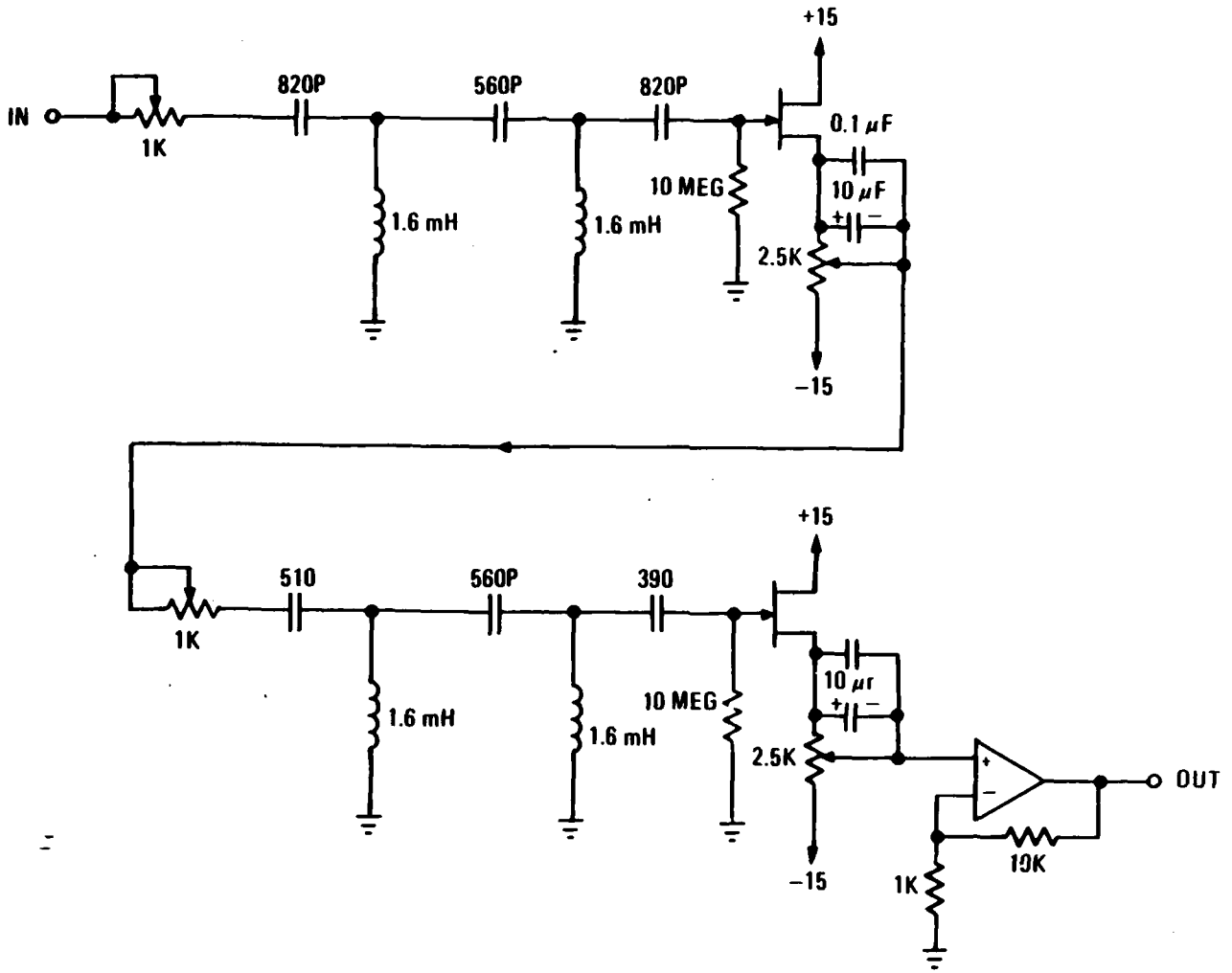

Fig. A-7. High-Pass Filter

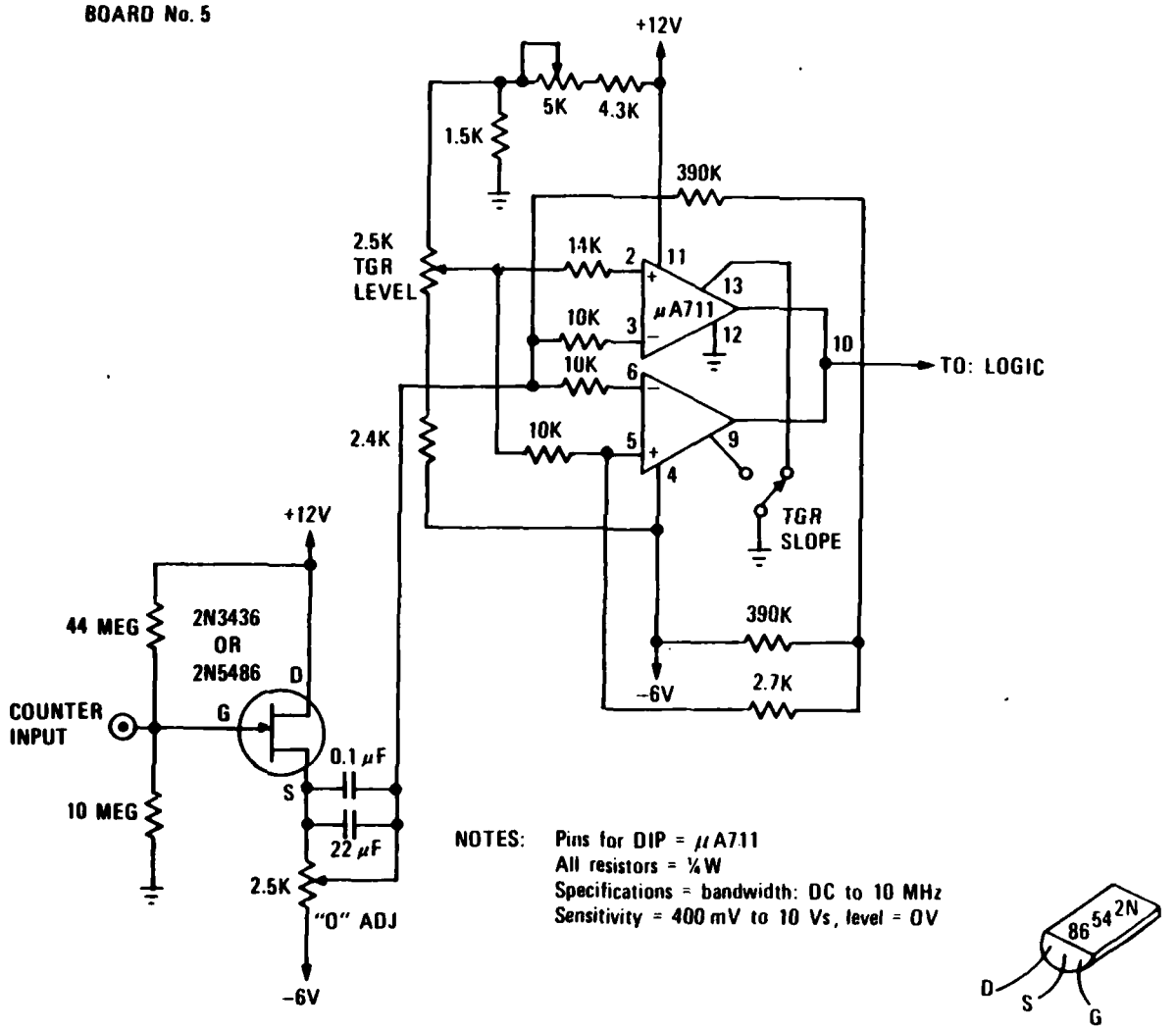

Fig. A-8. High-Speed Clipper

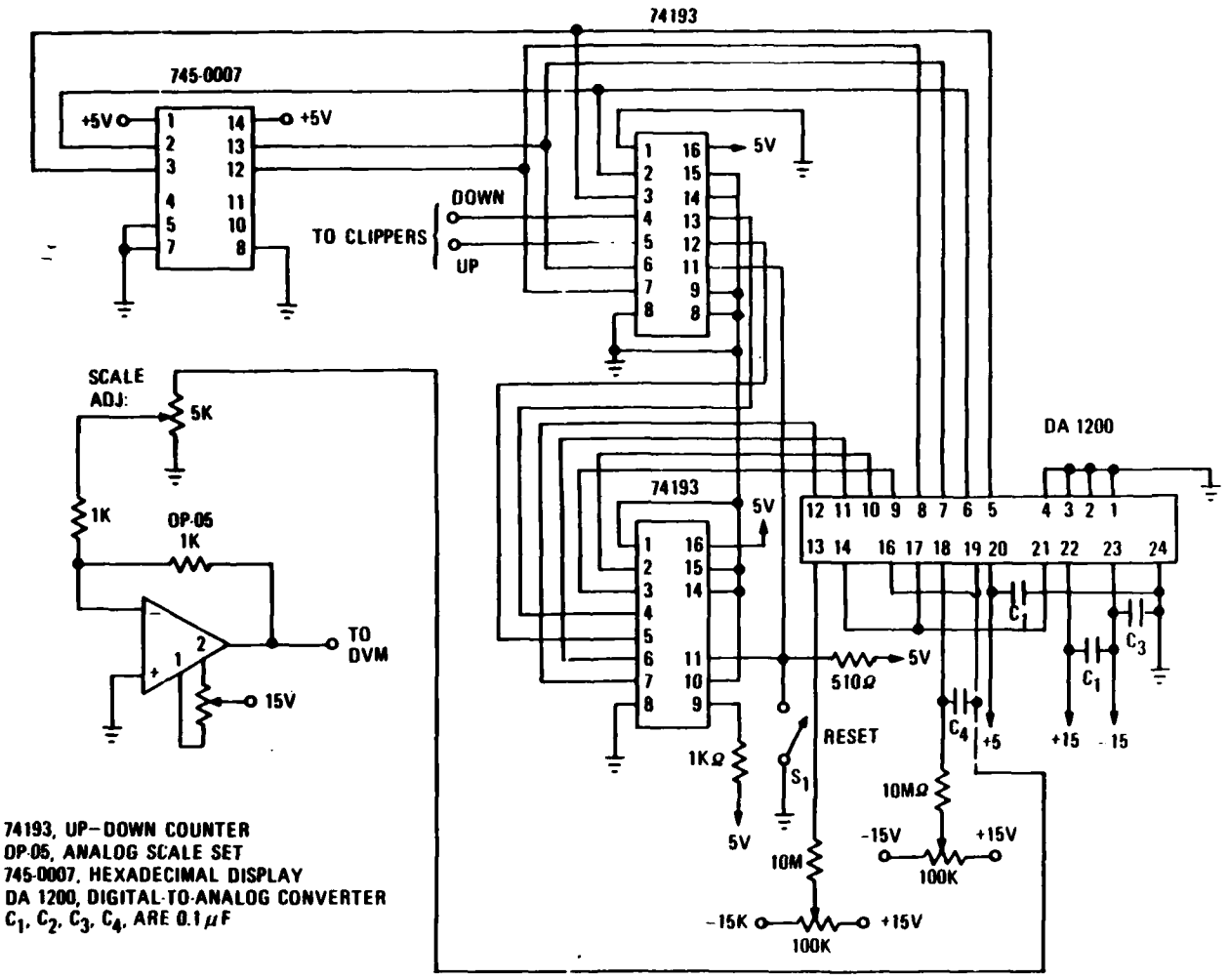

Fig. A-9. Up-Down Counter, Analog Scale Set, Hexadecimal Display, and Digital-to-Analog Converter

LIST OF SYMBOLS

c	speed of light in vacuum (m/s)
E,A	electric field amplitude (V/m)
E_z	applied field on electro-optic (E-O) modulator in z direction (V/m)
I	intensity (W/m^2)
J_n	Bessel functions
k	wave number (m^{-1})
ℓ	geometrical path length difference (m)
ℓ_c	length of E-O crystal transversed by beam (m)
n	index of refraction of optical medium
n_o	index of refraction of optical crystal path
r_{63}	component of electro-optic tensor (m/V)
V	voltage signal (V)
x,y,z	coordinates (m)
β	visibility
ε_o	free space permittivity (fd/m)
ω	frequency of light (sec^{-1})
ω_m	modulation frequency (sec^{-1})
λ	wavelength of (laser) beam in vacuo (m)
Γ	modulation index (rad)
ϕ	phase of interferometer (rad)

LABORATORY OPERATIONS

The Laboratory Operations of The Aerospace Corporation is conducting experimental and theoretical investigations necessary for the evaluation and application of scientific advances to new military concepts and systems. Versatility and flexibility have been developed to a high degree by the laboratory personnel in dealing with the many problems encountered in the Nation's rapidly developing space systems. Expertise in the latest scientific developments is vital to the accomplishment of tasks related to these problems. The laboratories that contribute to this research are:

Aerophysics Laboratory: Aerodynamics; fluid dynamics; plasmadynamics; chemical kinetics; engineering mechanics; flight dynamics; heat transfer; high-power gas lasers, continuous and pulsed, IR, visible, UV; laser physics; laser resonator optics; laser effects and countermeasures.

Chemistry and Physics Laboratory: Atmospheric reactions and optical backgrounds; radiative transfer and atmospheric transmission; thermal and state-specific reaction rates in rocket plumes; chemical thermodynamics and propulsion chemistry; laser isotope separation; chemistry and physics of particles; space environmental and contamination effects on spacecraft materials; lubrication; surface chemistry of insulators and conductors; cathode materials; sensor materials and sensor optics; applied laser spectroscopy; atomic frequency standards; pollution and toxic materials monitoring.

Electronics Research Laboratory: Electromagnetic theory and propagation phenomena; microwave and semiconductor devices and integrated circuits; quantum electronics, lasers, and electro-optics; communication sciences, applied electronics, superconducting and electronic device physics; millimeter-wave and far-infrared technology.

Materials Sciences Laboratory: Development of new materials; composite materials; graphite and ceramics; polymeric materials; weapons effects and hardened materials; materials for electronic devices; dimensionally stable materials; chemical and structural analyses; stress corrosion; fatigue of metals.

Space Sciences Laboratory: Atmospheric and ionospheric physics, radiation from the atmosphere, density and composition of the atmosphere, aurorae and airglow; magnetospheric physics, cosmic rays, generation and propagation of plasma waves in the magnetosphere; solar physics, x-ray astronomy; the effects of nuclear explosions, magnetic storms, and solar activity on the earth's atmosphere, ionosphere, and magnetosphere; the effects of optical, electromagnetic, and particulate radiations in space on space systems.

END

DATE
FILMED
4-82

DTIC